Trailing edge noise prediction for rotating serrated blades

S. Sinayoko*

Institute of Sound and Vibration Research, University of Southampton, UK

M. Azarpeyvand †

Faculty of Engineering, University of Bristol

B. Lyu ‡

Department of Engineering, University of Cambridge

Serrations have been widely studied in the case of stationary blades, as an efficient method for reducing trailing edge noise. However, most of the problems involving trailing edge noise are related to rotating blades and it is not known how rotation affects the efficiency of serrations. This paper tackles this problem using an efficient analytical model for predicting trailing edge noise radiation for rotating serrated blades. The model combines Howe's low Mach number isolated airfoil theory with Amiet's rotating airfoil technique. The paper also outlines a theory that generalizes Amiet's stationary airfoil theory to serrated trailing edges. Three different types of serrations – sinusoidal, sawtooth and slitted-sawtooth – are investigated for a model wind turbine blade element. The influence of the serrations width, depth, and slits, on noise radiation is compared to known results valid for stationary blades. The best serrations are narrow (relative to the boundary layer thickness) and deep. Rotation has been found to have little impact on the performance of serrations at low Mach numbers.

I. Introduction

Serrations offer an efficient way of reducing trailing edge noise, but little is known on how rotation affects their efficiency. This paper aims at quantifying the impact of rotation on the reduction in trailing edge noise

*Brunel Fellow, Royal Commission for the Exhibition of 1851, ISVR, University of Southampton, UK
†Lecturer, Royal Academy of Engineering Research Fellow, Faculty of Engineering, University of Bristol, UK
‡MPhil student, Department of Engineering, University of Cambridge

produced by serrations.

The use of trailing edge serrations for stationary aerofoils has been the subject of various studies over the past two decades. The first analytical model for the prediction of noise from serrated trailing edges was reported by Howe.[1–3] Assuming that the serrations do not change the hydrodynamic field near the trailing edge, Howe developed analytical models to study the trailing edge noise from a flat plate set at zero angle of attack to the mean flow with sawtooth[1] and sinusoidal[2] serration geometries. It was shown that the far-field noise can be significantly reduced at high frequency range if the serrations are shallow enough, relative to the boundary layer thickness at the trailing edge.

The effectiveness of noise reduction using trailing edge serrations have also been recently investigated experimentally.[4–7] It has been shown that significant noise reduction can be achieved using sawtooth serrations, provided that the geometrical parameters of the serration meet some specific conditions, as per Howe.[1,2] Experimental studies of the case of a flat plate with sawtooth serrations have also shown that the use of serrations can result in up to 3 dB noise reduction at low frequencies and also attenuation of up to 13 dB in blunt vortex shedding noise contribution at high frequencies.[7] The experimental data in the latter study had also indicated that the noise reduction capability of trailing edge serrations is related to their influence on the hydrodynamic field at the source location near the edge.

More recently, the application of complex periodic serrations, namely slitted, slitted-sawtooth, sinusoidal-sawtooth, etc, has been investigated analytically by Azarpeyvand et al[8] and experimentally by Gruber et al.[6,9] It has been shown[6] that slitted-sawtooth serrations can provide a good alternative to sawtooth serrations, offering similar levels of noise reductions while limiting the high frequency noise increase to no more than 1 dB. Random trailing edges has also been considered and was shown to provide reasonable levels of broadband noise reductions of up to 3 dB but no increase at high frequencies.[5] In this paper, the far-field noise spectrum for an isolated stationary blade will be calculated based on Howes original formulation[1–3] of trailing edge noise and the more recent formulation developed by Azarpeyvand et al.[8] for complex serration geometries.

As discussed above, noise reduction using trailing edge serrations for stationary blades has been the subject of numerous studies. However, the case of rotating blades with a serrated trailing edge has received little attention. The experimental study of Oerlermans[10] demonstrated that serrations did reduce trailing edge noise radiation for wind turbines. However, there has been no attempt to date at modelling rotating serrated blades analytically. The objective of this paper is to tackle this problem.

To model the power spectral density for sound radiating from a rotating serrated blade as measured by a stationary observer in the far field, we will combine the recent models developed by Azarpeyvand et al[8] with Amiet's approximate approach.[11–13] The advantage of Amiet's approach is that it allows one to predict

the power spectral density for a rotating blade provided that the power spectral density for a stationary blade is known. Thus, it can be combined with either an experimental database[14] or with semi-analytical models.[15–17] A recent study by Sinayoko et al[15] has validated Amiet's approach for trailing edge noise over a broad range of operating conditions and that approach has been used successfully for broadband noise from low speed axial fans by Rozenberg et al[18] and Kucukcoskun.[19] The objective will be to understand if the noise reduction observered in the case of stationary airfoils with serrated trailing edges still hold in the case of rotating blades. In particular, we will seek to understand whether the advanced trailing edges studied by Azarpeyvand et al[8] operate as efficiently for rotating blades.

The current approach is limited to low Mach number rotation due to the use of Howe's formulation.[1,2] In order to remove this constraint, we outline a new theory extending Amiet's trailing edge noise theory of stationary blades with straight edges to the case of sawtooth serrations.

The paper is organised as follows. The far-field noise prediction for a serrated stationary blade, with different periodic geometries, is explained Section II.A and II.B. The generalized Amiet model for serrated edges is presented in Section II.C. The trailing edge noise formulation for a rotating blade is summarized in Section III. Finally, section IV and V present respectively the numerical results and discussion.

II. Trailing edge noise theory for isolated aerofoils

A. General formulation for low Mach number flows

Consider a semi-infinite thin flat plate, at zero angle of attack to a low Mach number mean flow at speed U_0. The density and speed of sound of the medium are denoted by ρ_0 and c_0. A Cartesian coordinate system (x_1, x_2, x_3) is used to describe the problem, where x_1 is the chordwise direction, x_2 is the normal to the plane of the airfoil and x_3 is the spanwise direction. The flow is parallel to x_1 and is assumed to be turbulent. The trailing edge shape is defined as a function of the span-length, as $x_1 = \zeta(x_3)$ and is a pertiodic function of x_3 with zero mean.

The total pressure field $p(\boldsymbol{x}, \omega)$ can be represented in the form,

$$p(\boldsymbol{x}, \omega) = p_0(\boldsymbol{x}, \omega) + p_s(\boldsymbol{x}, \omega), \tag{1}$$

where p_0 is the incident pressure field that would be generated by the same turbulence vorticity field if the airfoil were absent, and p_s is the reflected and diffracted pressure field caused by the interaction of the incident field and the trailing edge. In the case of low Mach numbers and highly turbulent flows, the

governing equations of the incident (p_0) and scattered (p_s) fields are,

$$(\nabla^2 + \kappa_0^2)p_0 = Q(\boldsymbol{y}, \omega), \tag{2}$$

$$(\nabla^2 + \kappa_0^2)p_s = 0, \tag{3}$$

where $Q(\boldsymbol{y}, \omega)$ is the soruce term and is defined as the Fourier-time transform of Lighthill's quadrupole source, and $\kappa_0 = \omega/c_0$ is the acoustic wavenumber. Also, the incident pressure field within teh boundary layer can be expressed using the angular spectrum method, as

$$p_0(\boldsymbol{x}, \omega) = \int_{-\infty}^{+\infty} p_0(\boldsymbol{K}, \omega) e^{j[\boldsymbol{K}\cdot\boldsymbol{x} - \gamma(K)x_2]}\, d^2\boldsymbol{K}, \tag{4}$$

$$p_0(\boldsymbol{K}, \omega) = \frac{1}{(2\pi)^3} \int p_0(x_1, 0^+, x_3, \omega) e^{-j\boldsymbol{K}\cdot\boldsymbol{x}}\, d\boldsymbol{x}, \tag{5}$$

where $p_0(x_1, 0^+, x_3, \omega)$ is the boundary layer pressure field acting on the surface of the plate and can be measured experimentally using axial and lateral arrays of pressure transducers flush-mounted to the plate.[5]

The scattered pressure field, on the other hand, can be expressed in terms of a Kirchoff integral over the surface of the plate

$$p_s(\boldsymbol{x}, \omega) = \int_S \left([G(\boldsymbol{x}, \boldsymbol{y}, \omega)] \frac{\partial p_s}{\partial y_n}(\boldsymbol{y}, \omega) - p_s(\boldsymbol{y}, \omega) \left[\frac{\partial G}{\partial y_n}(\boldsymbol{x}, \boldsymbol{y}, \omega) \right] \right) dS(\boldsymbol{y}), \tag{6}$$

where $G(\boldsymbol{x}, \boldsymbol{y}, \omega)$ is an appropriate Green's function for sound diffraction by sharp edges, satisfying both the Kutta condition at the trailing edge, and the boundary condition on the surface of the plate, i.e.

$$\frac{\partial G}{\partial x_2} = 0, \qquad x_2 = 0^{\pm}, \quad x_1 < \zeta(x_3), \tag{7}$$

where the surface integral is taken over $-\infty < y_1 < \zeta(y_3)$ and along the span direction $-\infty < y_3 < \infty$, on the upper and lower surfaces. Due to the vanishing normal derivative, $\partial G/\partial y_n = 0$, over the surface of the airfoil, so Eq. (6) reduces to

$$p_s(\boldsymbol{x}, \omega) = \int_S [G(\boldsymbol{x}, \boldsymbol{y}, \omega)] \frac{\partial p_s}{\partial y_n}(\boldsymbol{y}, \omega)\, dS(\boldsymbol{y}) = \int_{-\infty}^{+\infty} dy_3 \int_{-\infty}^{\zeta(y_3)} \frac{\partial p_s}{\partial y_n}(\boldsymbol{x}, \omega)[G(\boldsymbol{x}, \boldsymbol{y}, \omega)]\, dy_1, \tag{8}$$

where y_n is the coordinate normal to the airfoil into the fluid at the source location. Also,

$$[G(\boldsymbol{x}, \boldsymbol{y}, \omega)] = G(\boldsymbol{x}, \boldsymbol{y}, \omega)|_{x_2=0^+} - G(\boldsymbol{x}, \boldsymbol{y}, \omega)|_{x_2=0^-}, \tag{9}$$

is the jump in the value of the Green's function across the plate surface, $y_2 = 0$.

In order to solve equation (8) analytically, one needs to find the scattered sound field near the trailing edge. Since the normal component of the velocity must vanish on the surface of the plate, i.e.

$$\frac{\partial p_0}{\partial y_2} + \frac{\partial p_s}{\partial y_2} = 0,$$

the pressure field in (8) can be expressed in terms of the incident pressure field. Also, it has been shown before that the incoming pressure field can be expressed in terms of the space-time Fourier transform of the turbulence *blocked pressure*, $p_b(x_1, x_3)$. The quantity p_b is basically the pressure that the same turbulent flow would produce on the plate (Ref.,[3] page 204) and is twice the pressure that the flow produces in the absence of the wall, i.e. $p_b = 2p_0$. Thus, the far-field pressure can now be found from

$$p_s(\boldsymbol{x}, \omega) = \frac{j}{2} \int_{-\infty}^{+\infty} dy_3 \int_{-\infty}^{\zeta(y_3)} dy_1 \int_{-\infty}^{+\infty} \gamma(K)[G(\boldsymbol{x}, y_1, y_3, \omega)] p_b(\boldsymbol{K}, \omega) e^{j[K_1 y_1 + K_3 y_3]} \, d^2\boldsymbol{K}, \tag{10}$$

where $\boldsymbol{K} = (K_1, 0, K_3)$ is the boundary layer turbulent wavenumber vector, and

$$\gamma(K) = \sqrt{\kappa_0^2 - |\boldsymbol{K}|^2} \quad \text{for} \quad \kappa_0 > |\boldsymbol{K}|,$$
$$\gamma(K) = j\sqrt{|\boldsymbol{K}|^2 - \kappa_0^2} \quad \text{for} \quad \kappa_0 < |\boldsymbol{K}|.$$

Using the change of variable $z_1 = y_1 - \zeta(y_3)$, the streamwise integration over y_1 in equation (10) can be simplified, as

$$p_s(\boldsymbol{x}, \omega) = \frac{j}{2} \int_{-\infty}^{+\infty} dy_3 \int_{-\infty}^{0} dz_1 \int_{-\infty}^{+\infty} \gamma(K)[G(\boldsymbol{y}, z + \zeta(y_3), y_3, \omega)] p_b(\boldsymbol{K}, \omega) e^{j[K_1 z_1 + K_3 y_3 + K_1 \zeta(y_3)]} \, d^2\boldsymbol{K}. \tag{11}$$

For a finite section of the airfoil wetted by the turbulent flow, the following relation between the surface pressure (p_s) and the blocked surface wavenumber-frequency spectrum, $P(K_1, K_3, \omega)$, can be used:

$$< p_b(K_1, K_3, \omega) p_b^*(K_1', K_3, \omega') > \approx \frac{l}{2\pi} P(K_1, K_3, \omega) \delta(K_1 - K_1') \delta(\omega - \omega'), \tag{12}$$

where the asterisk denotes complex conjugate, the angle brackets <> represents an ensemble average, l is the width of the wetted section ($-l/2 < y_3 < l/2$ and $l \gg \delta$), and $p_b(K_1, K_3, \omega)$ is the space-time Fourier transform of the turbulence blocked pressure $p_b(y_1, y_3, \omega)$, i.e. the pressure field developed beneath a boundary layer on a hard wall. The boundary layer forcing on the surface of the wall depends both on the temporal and spatial characteristics of the pressure and for locally plane surfaces the fluctuations can be considered statistically stationary in time and be expressed in terms of the wall pressure wavenumber-frequency spectrum. The wavenumber-frequency spectrum can be calculated by a Fourier transform of the

space-time correlation function of the wall pressure.[5] Various models have been developed for the surface pressure wavenumber-frequency spectrum. In this paper we shall use the model proposed by Chase flow low Mach number flows:

$$P(\boldsymbol{K},\omega) = \frac{C_m \rho_0^2 u_*^3 K_1^2 \delta^5}{[(K_1 - \omega/U)^2(\delta U/3u_*)^2 + (K\delta)^2 + \epsilon^2]^{5/2}}, \tag{13}$$

where $C_m = 0.1553$ is a non-dimensional coefficient, $U \approx 0.7U_0$ is the convection velocity, $\epsilon = 1.33$, δ is the boundary layer thickness, and $u_* = 0.03U_0$ is the friction velocity of the boundary layer upstream of the trailing edge. It is worth mentioning here that in the hydrodynamic domain, the surface pressure wavenumber-frequency spectrum exhibits a strong peak at $K_1 = \omega/U$, within the convective ridge area, see Fig 3.4.1 in Ref.,[3] and therefore equation (13) can be approximated by

$$P_c(K_1 = \omega/U, K_3, \omega) = C_m \rho_0^2 u_*^3 \delta^3 \frac{\widetilde{K}_1^2}{(\widetilde{K}_1^2 + \widetilde{K}_3^2 + \epsilon^2)^{5/2}}, \tag{14}$$

where the tilde denotes normalization by the boundary layer thickness δ, i.e. $\tilde{K} = K\delta$, in which case, any integral over the streamwise wavenumber K_1 can be assumed approximately equal to $P_c(K_1 = \omega/U, K_3, \omega)$. This will be used later for the calculation of the acoustic frequency spectrum using the surface pressure wavenumber frequency spectrum.

Finally, the acoustic pressure frequency spectrum $\Phi(\boldsymbol{x},\omega)$ can be found from the ensemble average of the acoustic pressure, as

$$\langle p_s(\boldsymbol{x},\omega) p_s^*(\boldsymbol{x},\omega')\rangle = \Phi(\boldsymbol{x},\omega)\delta(\omega - \omega'). \tag{15}$$

The above acoustic pressure frequency spectrum can be represented in the form

$$\Phi(\boldsymbol{x},\omega) = \frac{C_m(\rho_0 u_*^2)^2 l \delta^2}{\pi c_0 |\boldsymbol{x}|^2} \sin\psi \sin^2(\theta/2)\Psi(\omega), \tag{16}$$

where θ is the azimuthal angle measured from the flow direction x_1 in the (x_1, x_2) plane and ψ is the elevation angle measured from the x_3 axis, and $\Psi(\omega)$ is the non-dimensional edge noise spectrum.

B. Non-dimensional spectra for periodic trailing edges

The above trailing edge noise model can then be applied to different periodic trailing edge geometries. Figure 1 presents schematics of the different trailing edges considered in this paper. The nondimensional acoustic spectrum for some periodic geometries are reproduced here:[8]

1. Straight trailing edge

$$\Psi(\omega) = \psi(\widetilde{K}_1) \equiv \frac{\widetilde{K}_1^2}{[\widetilde{K}_1^2 + \epsilon^2]^2}, \tag{17}$$

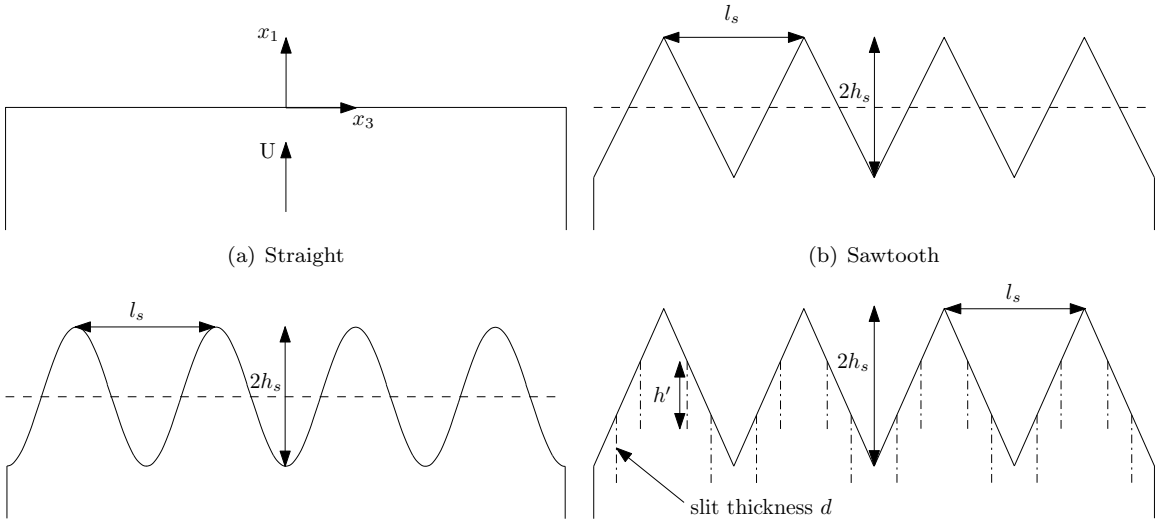

(a) Straight

(b) Sawtooth

(c) Sinusoidal

(d) Slitted sawtooth, for $p = 2$ slits per edge. Dash-dotted lines indicate the slits.

Figure 1: Schematic of the different trailing edges considered in this paper. The dashed lines indicate the position of the coordinate system in the chordwise direction.

where K_1 is the convective wavenumber ω/U and the tilde denotes normalization by δ. The nondimensional straight edge function ψ plays a key role in the serration models studied in this paper (see figure 1) as shown below.

2. Generic periodic serration of period l_s and amplitude $2h_s$

$$\Psi(\omega) = \sum_{n=-\infty}^{n=\infty} a_n(\widehat{K}_1)\psi(\widetilde{\rho}_n), \tag{18}$$

where a_n is a nondimensional modal amplitude, the hat denotes normalization by the serration semi-height h_s, and $\rho_n = \sqrt{K_1^2 + n^2 k_s^2}$ is a modal wavenumber that depends on the convective wavenumber and the serration wavenumber $k_s = 2\pi/l_s$. The modal amplitudes a_n used in this paper are given below:

(a) Sinusoidal

$$a_n(\widehat{K}_1) = J_n(\widehat{K}_1); \tag{19}$$

(b) Sawtooth

$$a_n(\widehat{K}_1) = 8\widehat{K}_1 \frac{[1 - (-1)^n \cos(2\widehat{K}_1)]}{(n^2\pi^2 - 4\widehat{K}_1^2)^2}; \tag{20}$$

(c) Slitted Sawtooth, with q slits of thickness d and depth h' on each edge

$$a_n(\widehat{K}_1) = \sum_{m=0}^{q} \left| \frac{x_n + \epsilon_m y_n}{2(n^2\pi^2 - 4\widehat{K}_1^2)} \right|^2, \tag{21}$$

where $\epsilon_m = 0$ if $m = 0$ and 1 otherwise,

$$x_n = n\pi(A+B) + 2\widehat{K}_1(B-A), \qquad y_n = n\pi(C+D) + 2\widehat{K}_1(D-C)e^{-i\widehat{K}_1 h'/h_s},$$
$$A = 1 - e^{i(n\pi+2\widehat{K}_1)(1-2q\overline{d})/(q+1)}, \qquad B = e^{-i(n\pi-2\widehat{K}_1)} - e^{-i(n\pi-2\widehat{K}_1)(1+2\overline{d})q/(q+1)},$$
$$C = e^{-i(n\pi+2\widehat{K}_1)(2\overline{d})} - 1, \qquad D = e^{-i(n\pi-2\widehat{K}_1)(1+2\overline{d})} - e^{-i(n\pi-2\widehat{K}_1)},$$

where $\overline{d} = d'/l_s$.

C. Towards a generalized Amiet model for a serrated trailing edge

Using Schwartzchild's method, Amiet managed to develop a model to predict the far-field noise generated by the interaction of a turbulent boundary layer with a straight trailing edge.[20] We propose to generalize Amiet's method to serrated trailing edges in this paper. The objective is to obtain a theory that is valid for any subsonic Mach number, as opposed to Howe's theory which is applicable only to low Mach numbers.

In order to apply the technique to solve the scattered field on the surface of an airfoil, a separation of the total pressure field into two different parts is necessary, say $p = p_0 + p_s$. The incident gust p_0 is based on the stationary statistical properties of the turbulent flow upstream of the trailing edge, which is given in the airfoil-fixed frame as,

$$p_0 = p_{0i} e^{i(K_1 x_1 + K_3 x_3)} e^{-i\omega t}, \tag{22}$$

where, p_{0i} is the magnitude of the gust, K_1 and K_3 denote the wavenumber of the gust in the x_1 and x_3 direction respectively. The convected wave equation in $\boldsymbol{x'}$ coordinate system is given by,[21]

$$\nabla^2 p_s - \frac{1}{c_0^2}\left(\frac{\partial}{\partial t} + U\frac{\partial}{\partial x_1}\right)^2 p_s = 0, \tag{23}$$

where U denotes the speed of uniform flow in x_1' direction and c_0 is the speed of sound in air. For a harmonic field $p_s = p_a e^{-i\omega t}$, using the coordinate transformation $y_1 = x_1 - H(x_3)$, $y_2 = x_2$ and $y_3 = x_3$ yields,[22]

$$\left(\beta^2 + H'^2(y_3)\right)\frac{\partial^2 p_a}{\partial y_1^2} + \frac{\partial^2 p_a}{\partial y_3^2} + \frac{\partial^2 p_a}{\partial y_2^2} - 2H'(y_3)\frac{\partial^2 p_a}{\partial y_1 \partial y_3} + \left(2iM_0 k - H''(y_3)\right)\frac{\partial p_a}{\partial y_1} + k^2 p_a = 0, \tag{24}$$

where $H(y_3)$ is the shape function of trailing edge serration, $M_0 = U/c_0$ and $\beta^2 = 1 - M_0^2$. The boundary conditions are given by

$$\begin{cases} p_a(y_1, 0, y_3) = -p_{0i} e^{i(K_1 y_1 + K_3 y_3)} e^{iK_1 H(y_3)}, & y_1 \geq 0 \\ \partial p_a(y_1, 0, y_3)/\partial y_2 = 0, & y_1 < 0. \end{cases} \tag{25}$$

Using separation of variable by means of a Fourier expansion of the surface pressure, one can express the acoustic pressure field, as

$$p_a(y_1, y_2, y_3) = \sum_{n=-\infty}^{\infty} P_n(y_1, y_2) e^{ik_{3n} y_3}, \tag{26}$$

where the modal wavenumber $k_{3n} = K_3 + nk_s$ combines the spanwise wavenumber K_3 with the serration wavenumber $k_s = 2\pi/l_s$. Substituting Eq. (26) into (24) yields

$$\left\{ \left(\beta^2 + H'^2(y_3)\right) \frac{\partial^2}{\partial y_1^2} + \frac{\partial^2}{\partial y_3^2} + \frac{\partial^2}{\partial y_2^2} - 2H'(y_3) \frac{\partial^2}{\partial y_1 \partial y_3} + (2iM_0 k - H''(y_3)) \frac{\partial}{\partial y_1} + k^2 \right\} \sum_{n=-\infty}^{\infty} P_n(y_1, y_2) e^{ik_{3n} y_3} = 0, \tag{27}$$

Multiplying Eq. (27) by $e^{-in'k_s}$ and integrating over one serration period in the spanwise direction y_3 gives

$$\left\{ \beta^2 \frac{\partial^2}{\partial y_1^2} + \frac{\partial^2}{\partial y_2^2} + 2ikM_0 \frac{\partial}{\partial y_1} + (k^2 - k_{3n'}^2) \right\} P_{n'} + \sum_{n=-\infty}^{\infty} \int_{-l_s/2}^{l_s/2} \left\{ H'^2(y_3) \frac{\partial^2}{\partial y_1^2} - (H''(y_3) + 2ik_{3n} H'(y_3)) \frac{\partial}{\partial y_1} \right\} P_n e^{i(n-n')k_s y_3} \, \mathrm{d}y_3 = 0. \tag{28}$$

The only way to obtain a decoupled equation that involves only one mode, say n', is when $H'(y_3)$ and $H''(y_3)$ are both constant. If the serration profile is a sawtooth, then H' is discontinuous and H'' contains Dirac δ functions at the root and tips of the serrations; all the modes are therefore coupled.

Coupled Equations

For a sawtooth profile, the coupling effect only involves the first derivative. For specific sawtooth with root-to-tip length $2h_s$ and wavelength l_s, let $\sigma = 4h_s/l_s$ denote the sawtooth slope. In that case $H'^2 = \sigma^2$ except at the corners, so the second partial derivative term in the integral in Eq. (28) is zero unless $n = n'$, and $H''(y_3) = -2\sigma\delta(y_3)$, so Eq. (28) reduces to

$$\left\{ L + (k^2 - k_{3n'}^2) \right\} P_{n'} = \frac{4\sigma}{l_s} \sum_{n-n'=odd} \left(1 - \frac{K_3 l_s + 2n\pi}{(n-n')\pi} \right) \frac{\partial P_n}{\partial y_1}. \tag{29}$$

where

$$L = \left\{ \left(\beta^2 + \sigma^2\right) \frac{\partial^2}{\partial y_1^2} + \frac{\partial^2}{\partial y_2^2} + 2ikM_0 \frac{\partial}{\partial y_1} \right\}. \tag{30}$$

To discretize the above equation, we assume that only the terms $-N \le n \le N$ need to be retained, i.e. $P_n = 0$ for all $|n| \ge N$. Let $\boldsymbol{P}$ denote the column vector

$$\mathbf{P} = \begin{pmatrix} P_{-N} & P_{-N+1} & \dots & P_{N-1} & P_N \end{pmatrix}^T, \tag{31}$$

then the coupled equation (29) can be discretized in the form

$$L\mathbf{P} = \mathbf{A}\mathbf{P} + \mathbf{B}\frac{\partial \mathbf{P}}{\partial y_1}, \tag{32}$$

where $\mathbf{A}$ and $\mathbf{B}$ denote the coefficients matrix of $\mathbf{P}$ and $\frac{\partial \mathbf{P}}{\partial y_1}$, respectively. The matrix $\mathbf{A}$ is diagonal, so if $\boldsymbol{B} \approx 0$ the modes are fully decoupled. One can solve for each P_n using the standard Schwartzschild technique.[18,32]

From the coupling equations, it can be seen that deeper serrations lead to large values of σ/l_s and so to stronger coupling. Since deep serrations are known to be more efficient at reducing noise it is likely that coupling, i.e. the scattering of modes into other modes, plays a major role in the physical process.

For low frequencies, we expect the solution to be dominated by mode 0 as the serrations are too small compared to the length scale of the fluctuations. In that case, we can therefore ignore higher order modes and treat the equation for mode 0 as fully decoupled. Thus, we expect coupling to become significant only as the frequency increases.

To solve the coupled equations at higher frequencies, we can use an iterative process whereby the solution is refined step by step by adding higher order terms (ramping up the amount of coupling until the solution converges). Since Schwartzschild's method is not applicable to inhomogenous equations, some further approximations are required at each step to obtain a solution analytically. In this paper, we will restrict ourselves to the 0-th order (decoupled) solution, but work is on-going to refine the solution for higher frequencies. The hope is that this process will uncover the mechanism by which sawtooth serrations achieve substantial reductions in trailing edge noise. Equation (29) suggests that the coupling encapsulated in matrix $\boldsymbol{B}$ must play a key role: the serrations affect the efficient transformation of hydrodynamic fluctuations into unsteady lift by scattering the modal amplitude towards multiple modes.

D. Boundary layer thickness model

Given a blade of chord length C, the boundary layer thickness will be estimated from the boundary layer displacement thickness as[25,26] $\delta = 8\delta^*$, where[27]

$$\delta^* = \begin{cases} C(24.3 + 0.6625\chi) \times 10^{-4}, & \text{if} \quad \chi \leq 4^\circ \\ C(26.95 + 0.6625(\chi - 4) + 0.3044(\chi - 4)^2 + 0.0104(\chi - 4)^3) \times 10^{-4}, & \chi > 4^\circ. \end{cases} \tag{33}$$

in terms of the angle of attack χ.

III. Trailing edge noise formulation for rotating blades

A. Instantaneous power spectral density for a rotating blade

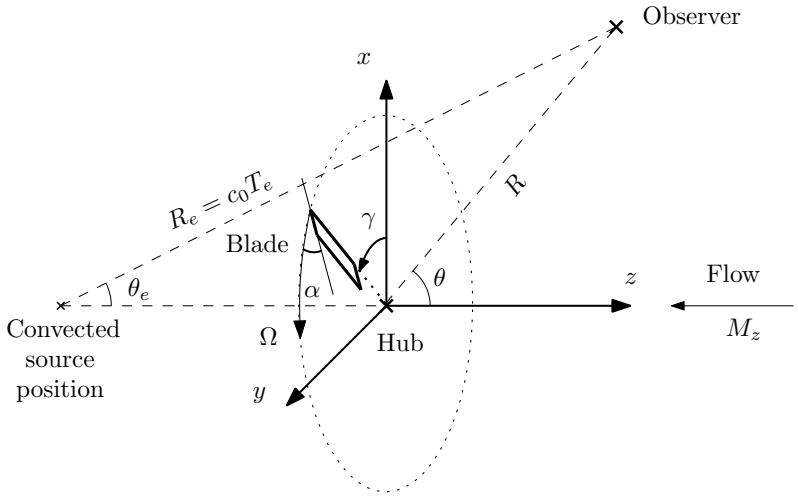

Figure 2: Stationary observer in a uniform flow. The reference frame is attached to the hub around which a blade element is rotating at angular velocity Ω. For an obsever in the far field, the source can be assumed to be located at the hub so the convected source position is as located downstream of the hub at $\mathbf{x_c} = -M_z c_0 T_e$.

Consider a rotating blade in a uniform flow. Trailing edge noise is emitted from the blade towards the observer who is assumed to be stationary. Since the blade is moving relative to the observer, the observer frequency ω is Doppler shifted compared to the source frequency ω'. The Doppler shift depends on the direction of the flow relative to the blade which varies with the azimuthal angle of the blade, so the power spectral density will be a function of the azimuthal angle of the blade, i.e. will be time dependent. A detailed account of the theory is presented in Sinayoko et al[15] but the main results are reproduced below.

We introduce a coordinate system (x, y, z) such that z is normal to the rotor plane and in the direction opposite to the flow velocity, as illustrated in figure 2 (wind turbine convention). Following Schlinker and Amiet's approach,[12] the blade is assumed to be in uniform rectilinear motion between emission time τ and reception time t. Using the conservation of power in a small frequency band near ω, the instantaneous PSD is given by[15]

$$S_{pp}(\mathbf{x_o}, t, \omega) = \frac{\omega'}{\omega} S'_{pp}(\mathbf{X}, \tau, \omega'), \tag{34}$$

where $\mathbf{x_o}$ is the observer position in a hub-fixed coordinates, and ω' and S'_{pp} are respectively the frequency and the instantaneous power spectral density in the reference frame of the blade. The above equation ignores the effect of the blade rotation between emission time and reception time; this means that the effect of acceleration is neglected which is a very good approximation up to very high subsonic Mach numbers.[16]

The observer position $\mathbf{X}$ is defined as

$$\mathbf{X}(\tau) = \underline{\mathbf{R_y}}(\alpha)\underline{\mathbf{R_z}}(\pi/2 - \alpha)(\mathbf{x} - \mathbf{x_p}(\tau)), \tag{35}$$

where α is the pitch angle, $\mathbf{x_p} \approx \mathbf{M_{BO}} c_0 T_e$ is the present source position (assuming that the source is emitted at the hub, which is valid for an observer in the far field) and is expressed in terms of the blade tangential (or rotational) Mach number $\mathbf{M_{BO}} \equiv M_t \hat{\boldsymbol{\gamma}}$ relative to the observer. $\underline{\mathbf{R_z}}$ and $\underline{\mathbf{R_y}}$ denote the rotation matrices about the z-axis and y'-axis respectively, with $y' = \underline{\mathbf{R_z}}(\pi/2 - \alpha)\mathbf{y}$. The propagation time T_e is obtained from $R_e \equiv c_0 T_e$, where R_e is the distance from the convected (or retarded) source position to the observer location:

$$R_e = \frac{R\left(-M_z \cos\Theta + \sqrt{1 - M_z^2 \sin^2\Theta}\right)}{1 - M_z^2}, \quad \text{(far field)}, \tag{36}$$

where $\Theta = \pi - \theta$ denotes the angle between the flow Mach number relative to the observer and $\mathbf{x_o}$ (see figure 2).

Finally, the source frequency ω' is related to the observer frequency ω through the Doppler shift[28]

$$\frac{\omega}{\omega'} = 1 + \frac{\mathbf{M_{BO}} \cdot \widehat{\mathbf{CO}}}{1 + (\mathbf{M_{FO}} - \mathbf{M_{BO}}) \cdot \widehat{\mathbf{CO}}} \quad \text{(far field)}, \tag{37}$$

where $\mathbf{M_{FO}} = -M_z \hat{\boldsymbol{z}}$ is the flow Mach number relative to the observer, and $\widehat{\mathbf{CO}} = \mathbf{CO}/|\mathbf{CO}|$ is the unit vector from the convected source position to the observer position (see figure 2).

The spectrum S'_{pp} in the reference frame of the blade can be computed from equation (16) with

$$S'_{pp}(\boldsymbol{X}, \tau, \omega') = \Phi(\boldsymbol{X}, \omega'), \tag{38}$$

where the flow velocity in Φ at time τ is defined as $U_0(\tau) = M_{FB}(\tau) c_0$. The isolated spectrum Φ is dependent on the non-dimensional spectrum Ψ associated with the geometry of the blade trailing edge. Ψ is given by equation (17) for a straight edge and (18) for a serrated edge.

B. Time averaged power spectral density

The time averaged PSD is obtained by averaging equation (34) over time t during one rotation of the rotor, and by making the change of variable $d\tau = (\omega/\omega')dt$ (by definition of the Doppler shift), which yields

$$\overline{S}_{pp}(\mathbf{x_o}, \omega) = \frac{1}{T} \int_0^T \left(\frac{\omega'}{\omega}\right)^2 S'_{pp}(\mathbf{X}, \tau, \omega')\, d\tau. \tag{39}$$

Note that the above integral can be replaced by an integral over azimuthal angle $0 < \gamma \leq 2\pi$, where $\gamma = \Omega\tau$:

$$\overline{S}_{pp}(\mathbf{x_o}, \omega) = \frac{1}{2\pi} \int_0^{2\pi} \left(\frac{\omega'}{\omega}\right)^2 S'_{pp}(\mathbf{X}, \gamma, \omega')\, d\gamma. \tag{40}$$

IV. Results

Figures 3 and 4 present the sound pressure level (SPL) as a function of observer elevation angle θ, as well as the sound power level (SPWL) as a function of non-dimensional frequency kC, for a serrated sawtooth wind turbine blade element. The wind turbine blade element has chord $C = 2$m, span $S = 7.25$m, pitch angle 10deg and rotational Mach $M_t = 0.165$ (so the chordwise Mach number is 0.167 and the flow Mach number is $M_z = 0.029$). The boundary layer thickness based on section D, and assuming 0 angle of attack, is 0.039m. The sound power level is computed using:[29]

$$W(\omega) = \frac{\pi R^2}{\rho_0 c_0} \int_0^{\pi} \overline{S}_{pp}(\theta, \omega) F(\theta) \sin\theta\, d\theta, \qquad F(\theta) = \frac{\beta^4 \sqrt{1 - M_z^2 \sin^2\theta}}{\left(\sqrt{1 - M_z^2 \sin^2\theta} + M_z \cos\theta\right)^2}, \tag{41}$$

and its level in decibels is relative to 1×10^{-12}.

Relative to the boundary layer thickness, the serrations are narrow in figure 3 ($l_s = 0.5\delta$) and wide in figure 4 ($l_s = 2\delta$). In each figure, the sound pressure level is plotted for serrations of varying height with h_s/δ equal to 0.5 (black squares), 1.0 (red diamonds) and 2.0 (blue circles), and the straight edge case (thin solid line) is included for comparison. The SPL is plotted in 3 separate figures at frequencies $kC = 1, 10$ (top row) and 100 (bottom left), and the SPWL is plotted for $1 \leq kC \leq 100$.

Figure 5 shows the SPWL for a sinusoidal profile, for a narrow serration relative to the boundary layer thickness ($l_s/\delta = 0.5$, left figure) or a wide serration ($l_s/\delta = 2$, right figure).

Figure 6 presents the SPWL for a slitted sawtooth profile. Figure 6(a) varies the number of slits per edge from 0 (black squares) to 6 (purple triangles), for a thickness ratio $\bar{d} = 0.02$. Figure 6(b) varies the slit thickness ratio $\bar{d}$ between 0.01 (black squares), 0.02 (red diamonds) and 0.04 (blue circles).

Figure 7 shows the reduction in sound power level $\Delta SPWL$ between a straight edge rotating wind turbine blade element, and a serrated sawtooth one, using several methods. The black squares correspond to Howe's model, while the solid line corresponds to the new model introduced in section C. It ignores the coupling and focuses on obtaining the 0-th order solution.

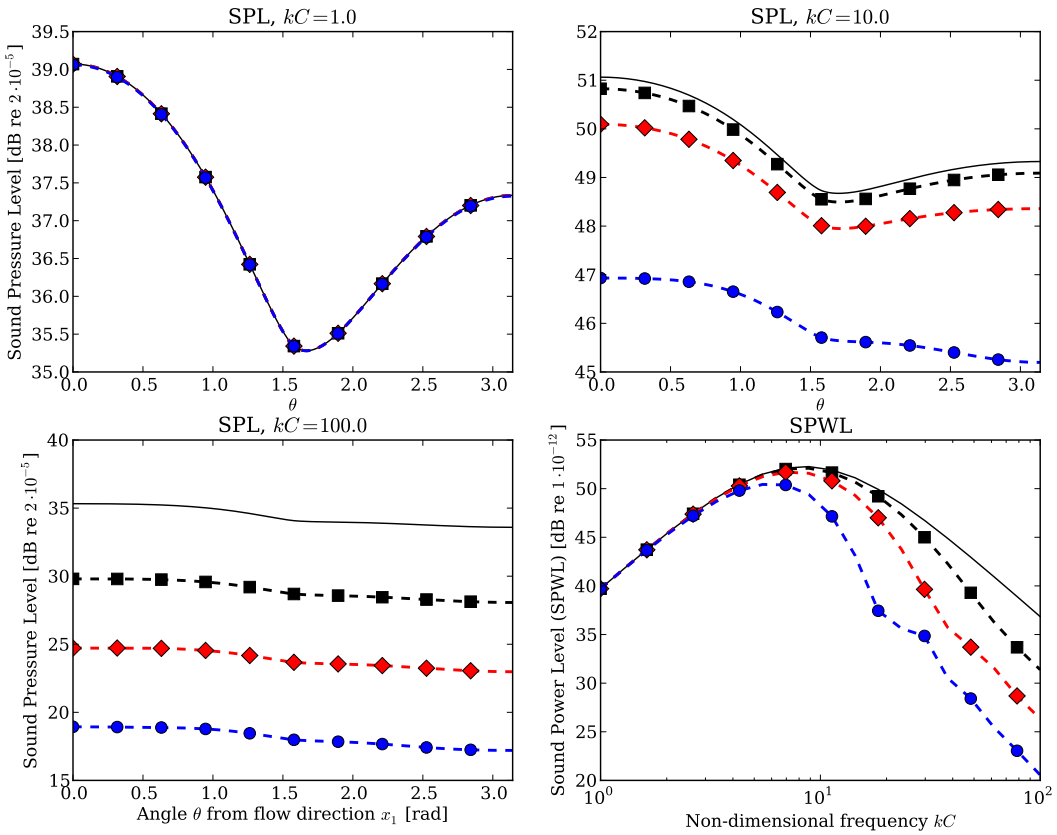

Figure 3: Sound Pressure Level directivity (SPL, top row and bottom left), and Sound Power Level (SPWL, bottom right) for a wind turbine blade element with sawtooth serrations (see figure 1). *The serrations are narrow* relative to the boundary layer thickness ($l_s/\delta = 0.5$). The black solid lines correspond to the straight edge reference case, while the dashed lines with markers are for serrated edges, with various values of the ratio h_s/l_s that defines the depth of the serrations: 0.5 (black squares), 1.0 (red diamonds) and 2.0 (blue circles). As for an isolated aerofoil,[8] the noise reduction increases with frequency and the depth of the serrations.

V. Discussion

Figure 3 shows that narrow sawtooth serrations reduce the sound pressure level over all angles, at high enough frequency $kC > 5$. The noise reduction increases with the sharpness of the serrations, i.e. with l_s/h_s. There is no noise reduction at low frequencies $kC < 5$ but, most importantly, there is no noise increase. On the contrary, figure 4 shows that wider serrations can increase the noise radiation at low frequencies (see top left figure and bottom right figure). The same conclusions hold for the sinusoidal profile, as shown in figure 5.

The noise performance of narrow and sharp serrations at low frequencies can be improved by introducing narrow slits within the serrations; this reduces the noise radiation significantly at low frequencies ($kC < 10$),

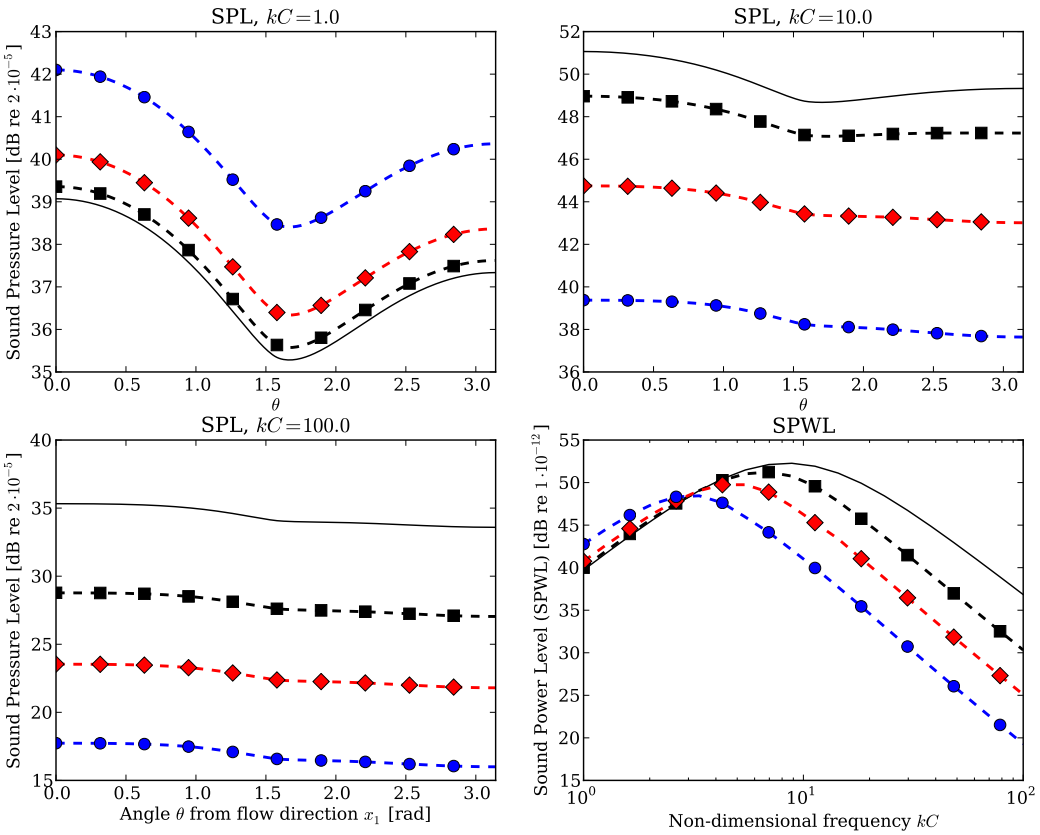

Figure 4: Sound Pressure Level directivity (SPL, top row and bottom left), and Sound Power Level (SPWL, bottom right) for a wind turbine blade element with sawtooth serrations (see figure 1). *The serrations are wide* relative to the boundary layer thickness ($l_s/\delta = 2$). The black solid lines correspond to the straight edge reference case, while the dashed lines with markers are for serrated edges, with various values of the ratio h_s/l_s that defines the depth of the serrations: 0.5 (black squares), 1.0 (red diamonds) and 2.0 (blue circles). As for an isolated aerofoil,[8] wide serrations relative to the boundary layer give a noise increase at low frequencies and a noise reduction at high frequencies. The noise reduction increases with frequency and the depth of the serrations.

and this effect increases with the number of slits. This comes at the cost of a smaller noise increase at higher frequencies ($kC > 10$).

The above observations are consistent with those observed by Gruber et al[6] and Azarpeyvand et al[8] for stationary blades: the optimal serrations for noise reduction are narrow relative to the boundary layer thickness ($l_s/\delta < 1$) and sharp ($h_s/l_s > 1$). This analytical study is also consistent with the noise reduction measured by Oerlermans[10] for serrated trailing edges. This is due to the dipolar directivity of trailing edge noise at low frequency, which can be seen on the top left directivity plot of figure 4; the directivity effects are mild and most of the effects of the serrations predicted for a stationary airfoil hold equally well for a rotating airfoil. More differences may occur for airfoils rotating at high speeds, which can not be studied

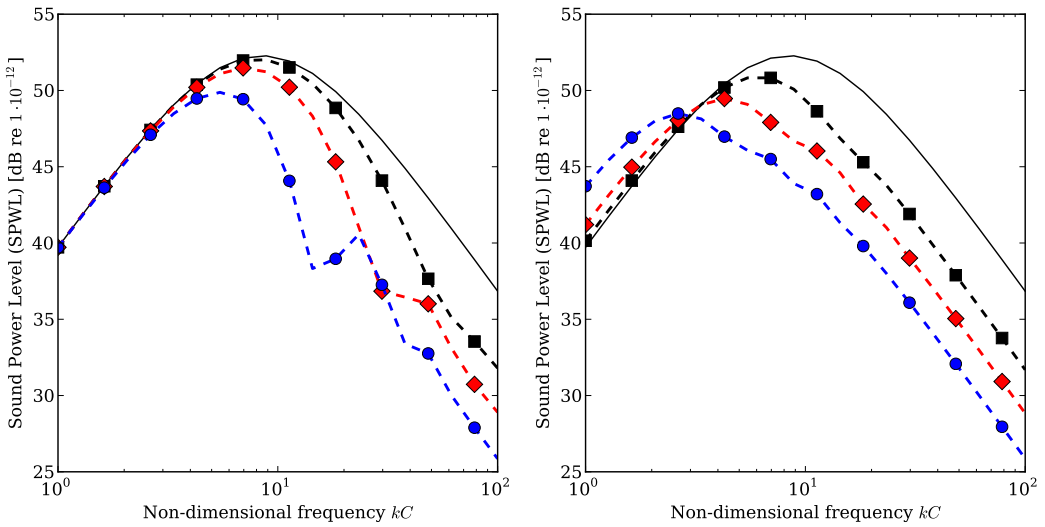

Figure 5: Sound power level as a function of frequency for a wind turbine blade element with sinusoidal serrations (see figure 1) for wide serrations ($l_s/\delta = 2$, right figure) or narrow serrations ($l_s/\delta = 0.5$, left figure). The black solid lines correspond to the straight edge reference case, while the dashed lines with markers are for serrated edges. The markers correspond to various values of the ratio h_s/l_s which defines the depth of the serrations: 0.5 (black squares), 1.0 (red diamonds) and 2.0 (blue circles). As for an isolated aerofoil,[8] wide serrations relative to the boundary layer give a noise increase at low frequencies and a noise reduction at high frequencies. The noise reduction is maximal for sharper serrations.

using Howe's model. Another reason for moving beyond Howe's model is that the levels of noise reduction it predicts are much higher than those measured experimentally.[6]

Figure 7 presents an estimate of the reduction in the sound power level due to sawtooth serrations. The reduction increases smoothly from 0 dB at $kC = 1$ to 15 dB at $kC = 100$. In practise, the noise reduction tends to be much lower,[5,6] usually less than 5 dB. The preliminary result for the generalized Amiet model of section C, shown as a solid line in 7, exhibits a noise increase for $kC < 11$, followed by significant noise reduction. The amount of noise reduction varies by up to 30 dB due to the presence of peaks that result from null values in the prediced PSD for the serrated edge. These peaks would be smoothed out were the coupling taken into account, bringing the predicted noise reduction down to values close to those observed experimentally.

VI. Conclusions

For blade elements rotating at low speed, such as found in wind turbines or cooling fans, the rotation has little impact on the noise reduction produced by serrations. Results obtained for a stationary blade can be readily applied to a rotating blade. In particular, the most effective serrations are narrow relative to the boundary layer thickness ($l_s < \delta$) and as deep as possible ($h_s > l_s$), and reduce noise at high enough

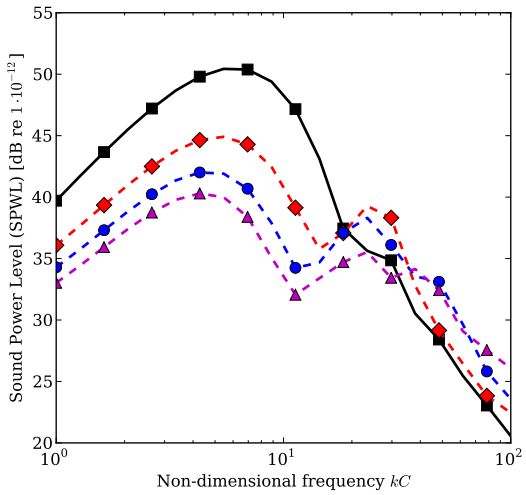

(a) Effect of the number of slits p: 0 (black squares), 2 (red diamonds), 4 (blue circles), 6 (purple triangles). The slit thickness is $c = 0.02$ and the slit depth is $h' = \delta$.

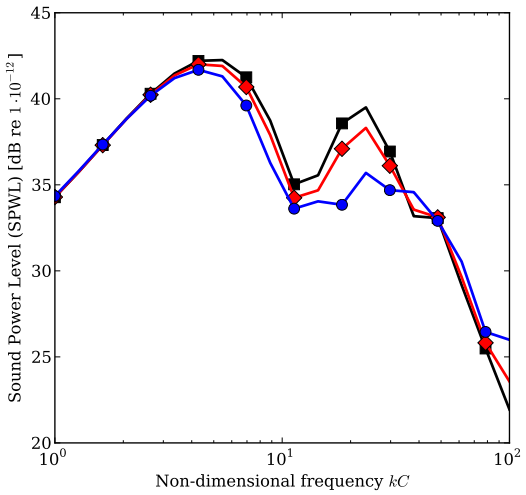

(b) Effect of the slit thickness c: 0.01 (black squares), 0.02 (red diamonds), 0.04 (blue circles). The number of slits is $p = 2$ and the slit depth is $h' = \delta$.

Figure 6: Sound power level as a function of frequency for a wind turbine blade element with slitted sawtooth serrations (see figure 1) for narrow and deep serrations: $l_s/\delta = 0.5$ and $h_s/l_s = 2$. As found for an isolated aerofoil,[8] the presence of slits provides noise reduction at low frequencies with a minor noise increase at high frequencies, and the noise reduction increases with the number of slits (left figure). The thickness of the slits has little effect on the noise reduction (right figure).

frequencies ($kC > 10$). Adding thin slits, with a thickness of the order of one percent of the serration period, provides additional noise reduction at low frequencies ($kC < 10$). Note that according to Gruber et al,[6] serrations tend to increase noise above a certain frequency, and that this noise increase is mitigated by the presence of slits within the serrations.

The current paper relies on Howe's theory[1–3,8] for a semi-infinite blades with serrated trailing edges, as well as on Amiet's approach[13,15] to extend Howe's theory to rotating blades. The accuracy of the model is limited by Howe's theory rather than Amiet's model. A novel theory of trailing edge noise for serrated edges, that is not limited to low Mach numbers and generalizes Amiet's trailing edge noise theory for stationary airfoils, has been outlined. It takes the form of a set of coupled equations between Fourier modes in the spanwise direction. The equations become decoupled only for a straight edge, where the theory reduces to Amiet's theory. Thus, the serrations are responsible for the amount of coupling in the equation and understanding this coupling is thought to be key to uncovering the physical mechanism by which serrations reduce trailing edge noise.

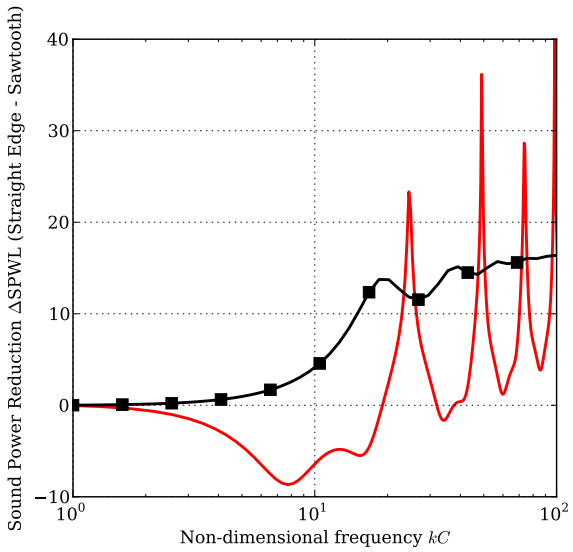

Figure 7: Reduction in sound power level $\Delta SPWL$, for trailing edge noise radiating from a rotating wind turbine blade element, between a straight edge and a sawtooth edge (with $l_s = 0.5\delta$ and $h_s/l_s = 2$). The square markers is based on Howe's models, the solid line on the 0-th order (decoupled) generalization to Amiet's model for serrated edges. Taking into account the effect of coupling is expected to smooth out the peaks in the generalized Amiet model bring the results closer to experimental measurements than Howe's model.

Acknowledgements

The first author (SS) wishes to gratefully acknowledge the financial support of the Royal Commission for the Exhibition of 1851 and of the University of Southampton. The second author (MA) would like to acknowledge the financial support of the Royal Academy of Engineering. The third author (BL) would like to acknowledge the financial support provided by Cambridge Overseas Trust and Agricultural Bank of China.

References

[1]Howe, M. S., "Noise produced by a sawtooth trailing edge," *The Journal of the Acoustical Society of America*, Vol. 90, No. 1, July 1991, pp. 482–487.

[2]Howe, M., "Aerodynamic noise of a serrated trailing edge," *Journal of Fluids and Structures*, Vol. 5, No. 1, Jan. 1991, pp. 33–45.

[3]Howe, M., *Acoustics of fluid-structure interactions*, Cambridge University Press, Cambridge [etc.], 1998.

[4]Gruber, M., Joseph, P., and Chong, T. P., "Experimental Investigation of Airfoil Self Noise and Turbulent Wake Reduction by the use of Trailing Edge Serrations," American Institute of Aeronautics and Astronautics, June 2010.

[5]Gruber, M., *Airfoil noise reduction by edge treatments*, phd, University of Southampton, Feb. 2012.

[6]Gruber, M., Joseph, P., and Azarpeyvand, M., "An experimental investigation of novel trailing edge geometries on airfoil trailing edge noise reduction," American Institute of Aeronautics and Astronautics, May 2013.

[7]Moreau, D. J. and Doolan, C. J., "Noise-Reduction Mechanism of a Flat-Plate Serrated Trailing Edge," *AIAA Journal*, Vol. 51, No. 10, Oct. 2013, pp. 2513–2522.

[8]Azarpeyvand, M., Gruber, M., and Joseph, P., "An analytical investigation of trailing edge noise reduction using novel serrations," American Institute of Aeronautics and Astronautics, May 2013.

[9]Gruber, M., Joseph, P., and Azarpeyvand, M., "Blade for a rotating machine," June 2013, International Classification F03D1/06, F01D5/14;.

[10]Oerlemans, S., Fisher, M., Maeder, T., and Kgler, K., "Reduction of wind turbine noise using optimized airfoils and trailing-edge serrations," *AIAA journal*, Vol. 47, No. 6, 2009, pp. 14701481.

[11]Amiet, R. K., "Noise Produced by Turbulent Flow into a Propeller or Helicopter Rotor," *AIAA Journal*, Vol. 15, No. 3, March 1977, pp. 307–308.

[12]Schlinker, R. H. and Amiet, R. K., "Helicopt," Tech. Rep. 1, NASA Contractor Report 3470, Jan. 1981.

[13]Amiet, R. K., "Leading and Trailing Edge Noise from a Helicopter Rotor," Tech. rep., UTRC Report 86-53, 1986.

[14]Brooks, F., Pope, D. S., and Marcolini, A., "Airfoil Self-Noise and Prediction," Tech. rep., NASA Reference Publication 1218, 1989.

[15]Sinayoko, S., Kingan, M., and Agarwal, A., "Trailing edge noise theory for rotating blades in uniform flow," *Proceedings of the Royal Society A: Mathematical, Physical and Engineering Science*, Vol. 469, No. 2157, Sept. 2013, pp. 20130065.

[16]Sinayoko, S., Kingan, M., and Agarwal, A., "On the effect of acceleration on trailing edge noise radiation from rotating blades," American Institute of Aeronautics and Astronautics, May 2013.

[17]Blandeau, V. P. and Joseph, P. F., "On the validity of Amiet ' s model for propeller trailing-edge noise," *Fluid Dynamics*, 2010, pp. 1–17.

[18]Rozenberg, Y., Roger, M., and Moreau, S., "Rotating Blade Trailing-Edge Noise: Experimental Validation of Analytical Model," *AIAA Journal*, Vol. 48, No. 5, May 2010, pp. 951–962.

[19]Kucukcoskun, K., Christophe, J., Schram, C., and Tournour, M., "A Semi-Analytical Approach on the Turbulence Interaction Noise of A Low-Speed Axial Fan Including Broadband Scattering," American Institute of Aeronautics and Astronautics, June 2011.

[20]Amiet, R., "High frequency thin-airfoil theory for subsonic flow," *AIAA Journal*, 1976.

[21]Amiet, R., "Noise due to turbulent flow past a trailing edge," *Journal of Sound and Vibration*, Vol. 47, 1976, pp. 387–393.

[22]Roger, M., Schram, C., and Santana, L. D., "Reduction of Airfoil Turbulence-Impingement Noise by Means of Leading-Edge Serrations and/or Porous Materials," *arc.aiaa.org*, 2013, pp. 1–20.

[23]Curle, N., "The Influence of Solid Boundaries upon Aerodynamic Sound," *Proceedings of the Royal Society A: Mathematical, Physical and Engineering Sciences*, Vol. 231, No. 1187, Sept. 1955, pp. 505–514.

[24]Amiet, R., "Acoustic radiation from an airfoil in a turbulent stream," *Journal of Sound and Vibration*, Vol. 41, 1975, pp. 407–420.

[25]Rozenberg, Y., *Modelisation analytique du bruit a erodynamique a large bande des machines tournantes : utilisation de calculs moyennes de mecanique des fluides*, Ph.D. thesis, 2007.

[26]Blandeau, V., *Aerodynamic Broadband Noise from Contra-Rotating Open Rotors*, Ph.D. thesis, University of Southampton, 2011.

[27]Chou, S. and George, A. R., "Effect of angle of attack on rotor trailing-edge noise," *AIAA journal*, Vol. 22, 1984, pp. 1821–1823.

[28]Amiet, R. K., "Frame of Reference Considerations for the Forward Flight Noise Problem," Tech. rep., UARL Report N212775-1, 1974.

[29]Sinayoko, S., Joseph, P., and McAlpine, A., "Multimode radiation from an unflanged, semi-infinite circular duct with uniform flow," *The Journal of the Acoustical Society of America*, Vol. 127, 2010, pp. 2159.

[30]Amiet, R., "Noise due to turbulent flow past a trailing edge," *Journal of Sound and Vibration*, Vol. 47, No. 3, Aug. 1976, pp. 387–393.

[31]Amiet, R. K., "High frequency thin-airfoil theory for subsonic flow," *AIAA Journal*, Vol. 14, 1976, pp. 1076–1082.

[32]Roger, M. and Moreau, S., "Back-scattering correction and further extensions of Amiet's trailing-edge noise model. Part 1: theory," *Journal of Sound and Vibration*, Vol. 286, No. 3, Sept. 2005, pp. 477–506.

[33]Roger, M., Schram, C., and De Santana, L., "Reduction of Airfoil Turbulence-Impingement Noise by Means of Leading-Edge Serrations and/or Porous Material," American Institute of Aeronautics and Astronautics, May 2013.